

Research Article / Araştırma Makalesi

Preliminary design and analysis of an afterburner module / Bir art yakıcı modülünün ön tasarımı ve analizi

 Muhammed Cuma Sönmez¹,  Mustafa Karabacak^{2*},  Muammer Özgören²

¹ Necmettin Erbakan University, Mechanical Engineering Department, Konya, Türkiye

² Necmettin Erbakan University, Aeronautical Engineering Department, Konya, Türkiye

Received

November 16, 2023

Revised

December 12, 2023

Accepted

December 13, 2023

Keywords

Afterburner

Vee-gutter

GE J79 engine

Thrust

ABSTRACT

In this study, design calculations and calculations of afterburner used in jet engines are presented by evaluating the results of analytical and computational analysis. Afterburner inlet values of 1050 K temperature, 300 kPa pressure and 3.6 kg/s mass flow rate are taken as the design conditions. Maximum length and diameter are 500 mm and 200 mm, respectively, for the sections to be designed as length constraints within the scope of the conceptual design. The two-ring vee-gutter has 1.33 cm in diameter and 4.25 cm high. Jet A fuel is assumed to be injected into the core flow (90 degrees) from the spray bars. The spray is mounted in line with the vee-gutter to optimize the mixing of the flow. Analyses are performed for 4 cm between the spray bar and the vee-gutter. For the study, the GE J79 engine was examined from the literature and taken as a basis for the aerodynamic transition section design. Within the scope of TEKNOFEST 2023 Jet Engine Design Competition, a preliminary design of an afterburner module that can produce 700 pounds of thrust and has a life capacity of 25 hours should be realized in line with the design requirements and constraints. In the light of geometric constraints, one-dimensional combustion calculations of the module are made, and the parts are modelled using the relevant SolidWorks CAD program and these modelled parts are then transferred to ANSYS™ environment and the results and analyses are verified. The afterburner module flow analysis software program ANSYS™ is used to analyse the afterburner operation in both cold operating ranges (i.e. without combustion) using compressible, viscous and standard k-epsilon turbulence model. As a result, the effect of afterburner length on combustion performance is found to be significant. As a result of the calculations, afterburner length is found as 28.14 cm. It is found that the combustion efficiency is 81.5% and the temperature can be increased from 1050 K to 2044 K. The total pressure loss is 14.96% as pressure drop due to the geometric parameters and heat addition. The blockage ratio calculated due to the use of vee-gutter geometry is the most important parameter in the pressure drop. It is found that the jet engine producing 670 lbs (2981 N) of thrust when the afterburner is not working whereas it can provide a significant amount of power increment at the expense of a 50% increase in specific fuel consumption when the afterburner is active as well as providing a 738 lbs (3238 N) with a 10.1% thrust increase. The reason of the enhancement is mainly coming from the mixing effect of the vee-gutter on the flow structure.



ÖZET

Anahtar Kelimeler

Art yakıcı
Vee-gutter
GE J79 motor
İtki

Production and hosting by
[Turkish DergiPark](http://TurkishDergiPark.com). This is an
open access article under the
CC BY-NC license
(<https://creativecommons.org/licenses/by-nc/4.0/>).



Bu çalışmada, jet motorlarında kullanılan art yakıcının tasarım hesapları ve hesaplamaları analitik ve hesaplamalı analiz sonuçları değerlendirilerek sunulmuştur. Art yakıcı giriş değerleri olarak 1050 K sıcaklık, 300 kPa basınç ve 3,6 kg/s kütleli debi tasarım şartları olarak alınmıştır. Kavramsal tasarım kapsamında uzunluk kısıtı olarak tasarlanacak kesitler için maksimum uzunluk ve çap sırasıyla 500 mm ve 200 mm'dir. İki halkalı oluk 1,33 cm çapında ve 4,25 cm yüksekliğindedir. Jet A yakıtının püskürtme çubuklarından çekirdek akışına (90 derece) enjekte edildiği varsayılmaktadır. Sprey, akışın karışımını optimize etmek için damar oluşu ile aynı hızda monte edilmiştir. Analizler püskürtme çubuğu ile oluk arasındaki 4 cm için gerçekleştirilmiştir. Çalışma için GE J79 motoru literatürden incelenmiş ve aerodinamik geçiş kesiti tasarımı için temel alınmıştır. TEKNOFEST 2023 Jet Motoru Tasarım Yarışması kapsamında tasarım gereksinimleri ve kısıtları doğrultusunda 700 libre itki üretebilen ve 25 saat ömür kapasitesine sahip bir art yakıcı modülün ön tasarımının gerçekleştirilmesi gerekmektedir. Geometrik kısıtlar ışığında modülün tek boyutlu yanma hesapları yapılarak ilgili SolidWorks CAD programı kullanılarak parçalar modellenir ve modellenen bu parçalar daha sonra ANSYS™ ortamına aktarılarak sonuçlar ve analizler doğrulanır. Art yakıcı modülü akış analizi yazılım programı ANSYS™, sıkıştırılabilir, viskoz ve standart k-epsilon türbülans modeli kullanılarak her iki soğuk çalışma aralığında (yani yanma olmadan) art yakıcı çalışmasını analiz etmek için kullanılmıştır. Sonuç olarak, art yakıcı uzunluğunun yanma performansı üzerindeki etkisinin önemli olduğu bulunmuştur. Hesaplamalar sonucunda art yakıcı uzunluğu 28,14 cm olarak bulunmuştur. Yanma veriminin %81,5 olduğu ve sıcaklığın 1050 K'den 2044 K'ye çıkarılabileceği bulunmuştur. Geometrik parametreler ve ısı ilavesi nedeniyle basınç düşüşü olarak toplam basınç kaybı %14,96'dır. Damar-oluk geometrisinin kullanımına bağlı olarak hesaplanan blokaj oranı basınç düşüşündeki en önemli parametredir. Art yakıcı çalışmadığında 670 lbs (2981 N) itki üreten jet motorunun, art yakıcı aktif olduğunda özgül yakıt tüketiminde %50'lik bir artış pahasına önemli miktarda güç artışı sağlayabildiği ve %10,1'lik bir itki artışı ile 738 lbs (3238 N) itki sağladığı tespit edilmiştir. Bu artışın nedeni, esas olarak damar oluşunun akış yapısı üzerindeki karıştırma etkisinden kaynaklanmaktadır.

* Corresponding author, e-mail: mkarabacak@erbakan.edu.tr

Nomenclature

Abbreviation		Greek Letters	
K	Kelvin	π	Total Pressure Ratio [-]
kPa	Kilopascal	γ	Specific Heat Ratio [-]
m	Meter	τ	Total Temperature Ratio [-]
Symbols		ϵ	The "k- ϵ " Turbulence Model Coefficient
a	Sound Speed [m/s]	κ	The "k- ϵ " Turbulence Model Coefficient
B	Blockage Ratio [-]	Subscripts	
c	Specific Heat [J/kg]	1,2	Afterburner Zone Expressed by Engine Nomenclature
c_{1,2}	The "k- ϵ " Turbulence Model Coefficients	AB	Afterburner
C_D	Drag coefficient	f	Fuel
m	Mass Flow Rate [kg/s]	p	Constant Pressure
M	Mach number [-]	t	Total
P	Pressure [N/m ²]		
T	Thrust [N]		

1. Introduction

Afterburner application is a tool developed to adapt the aircraft to different flight missions [1-3]. By using this tool, it is possible to increase the manoeuvrability of a fighter aircraft in a dogfight by increasing the thrust [4,5], to increase the thrust of a bomber to enable it to quickly move away from enemy territory [6], to enable the aircraft to take off from short runways such as aircraft carriers, etc. This application is used extensively in military aviation



today [7,8]. During combustion in the combustion chamber, part of the oxygen of the air flow is used to prevent the aerodynamic structure of the turbine blades from deforming beyond certain limits with temperature [9,10]. Advances in cooling technology, application of thermal protection coatings and super alloy technology have increased the turbine inlet temperature [11,12], but the conditions are still far from the stoichiometric combustion limit of fuels [13,14]. For all these reasons, oxygen-rich air flow continues to exist at the nozzle inlet today. Increasing the thrust by afterburner application is based on the combustion of the oxygen-rich air flow by fuel injection [15,16]. This allows for a higher total temperature of air flow at the nozzle inlet. With afterburner combustion, losses due to the combustion occur in total pressure [17,18]. However, in afterburner applications, the thrust-reducing effect of the total pressure drop is compensated by the thrust-increasing effect of the increase in total temperature, and even an increase in impulse is achieved by obtaining a higher velocity flow at the nozzle exit. Today, afterburner design is expected to minimize total pressure losses and to maximize the total temperature at the nozzle inlet [19,20]. In addition to all these expectations, minimizing the negative effects of afterburner application on engine design by increasing length and weight are also seen as a design expectation [21]. With the development of afterburner design, the maximum total temperature increase with minimum pressure loss can be realized with the lowest possible length and weight increase in the engine [22]. With development of new fuels used in afterburner combustion engine weight and length penalty can be reduced [23]. On the other hand, using new materials weight penalty can be reduced in afterburner design similarly [24]. Motivation of the study is to show the afterburner effect on the flow structure and thrust for a special GE J79 engine case. Afterburner design having parametric analysis, CFD analysis and CAD drawing of afterburner module is firstly investigated together in more detailed than previous studies in literature.

2. Afterburner Design and Approach

2.1. On-design point

In the current design, the aim is primarily to obtain a working afterburner meeting the thrust performance requirement. The criteria for the preliminary design conditions of the short afterburner for the TEKNOFEST 2023 competition turbojet engine are expressed. This module consists of a diffuser, circular combustion chamber with 24 injectors, 2-ring vee-gutter, cooling liner and nozzle. The design point parameters of the core engine are provided by TEKNOFEST, and these parameters are used in the afterburner design.

Table 1. On-design point parameters.

Parameter	Value
Afterburner Inlet Total pressure [kPa]	300
Afterburner Inlet Total Temperature [K]	1050
Mass flow Rate [kg/s]	3.6
Inlet Gas Composition [-]	$O_2: 5.05 \times 10^{-3}$
	$N_2: 2.66 \times 10^{-2}$
	$H_2O: 1.34 \times 10^{-3}$
	$CO_2: 1.40 \times 10^{-3}$
Cooling Air Temperature [K]	540
Cooling Air Pressure [kPa]	720
Fuel Type	Jet A

Low combustion efficiency is not a major obstacle to thrust increase because even if the amount of fuel leaving the afterburner without combustion is high, the required fuel can be sprayed in the afterburner with the engine control system and the temperature limit restrained by the material strength at the afterburner exit can be reached. However, the increase in pressure losses reduces the thrust. For this reason, the afterburner design is to realize a



design that will provide the required combustion while reducing pressure losses and achieving this goal. Afterburner total pressure ratio is expressed in Equation 1 [25].

$$\pi_{AB} = 1 - \frac{(\tau_{AB} - 1) + C_D \times B}{1 + \frac{2}{\gamma \times M_1^2}} \quad (1)$$

where

- τ_{AB} : Afterburner total temperature ratio ($\tau_{AB}=1.905$ (Design point))
- M_1 : Afterburner inlet Mach number (Depending on the design of the mixer, the turbine exits flow Mach number and bypass channel exit flow Mach number)
- B: $B= D/H$ (Afterburner geometric parameters D and H are expressed in Figure 1)
- C_D : The drag coefficient.

The afterburner of the mixer should have a design that will allow us to achieve the afterburner design objectives (i.e. a design that will allow low pressure loss and combustion).

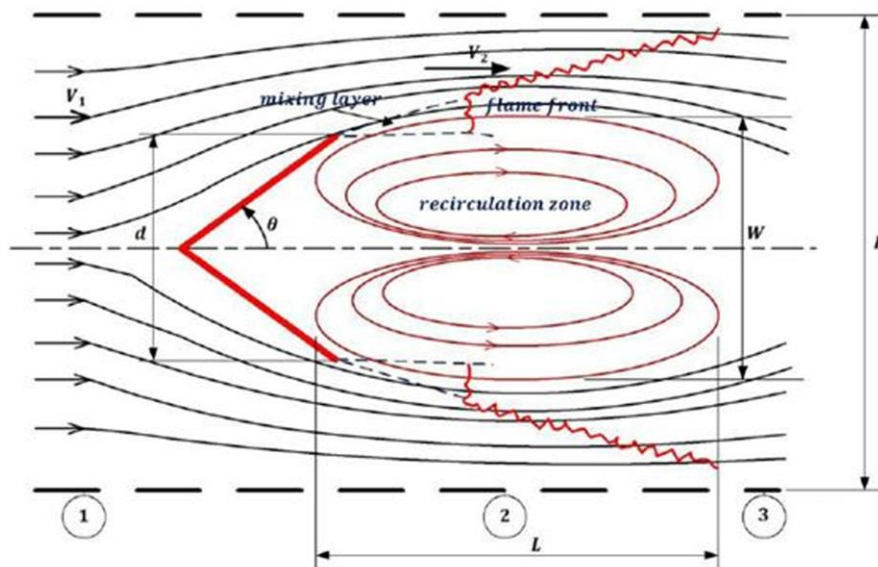


Fig. 1. Afterburner design parameters [25].

The drag coefficient and vee-gutter are expressed in igniter designs depending on the afterburner geometric parameters as shown below [25].

$$C_D = \frac{H}{D} \frac{W^2}{(H-W)^2} \quad (2)$$

The expressed geometric parameters are shown in Figure 1. The following relation is proposed between the geometrical parameters expressed in Cornell's graphical analysis [25].

$$\frac{W}{H} \approx B + (1 - \sqrt{B}) \sqrt{B \times \sin\left(\frac{\theta}{2}\right)} \quad (3)$$

The parameter H, depending on the number of afterburner igniters and afterburner diameter, is expressed as follows:



$$H \approx \frac{D_{AB}}{2 \times N_A} \tag{4}$$

The afterburner duct diameter should not exceed the maximum engine diameter. Increasing the number of afterburner rings reduces the afterburner length, but on the other hand increases pressure losses and reduces the residence time of the air-fuel mixture in the afterburner, thus adversely affecting combustion efficiency.

Reducing the number of afterburner rings increases the afterburner length, improves combustion efficiency, and increases the residence time of the fuel-air mixture but reduces pressure losses. However, the number of afterburners cannot be reduced beyond a certain number since the upper limit of the afterburner channel diameter is limited to the maximum diameter of the engine and the lowest value that the H parameter can take is limited for combustion to take place. The minimum value that the H parameter can take to determine the number of afterburners is expressed below [26].

$$H_{min} = 1.042 \times U_1 \times t_{BO} \tag{5}$$

t_{BO} : Blow out time.

U_1 : Afterburner inlet flow velocity (Depending on mixer design)

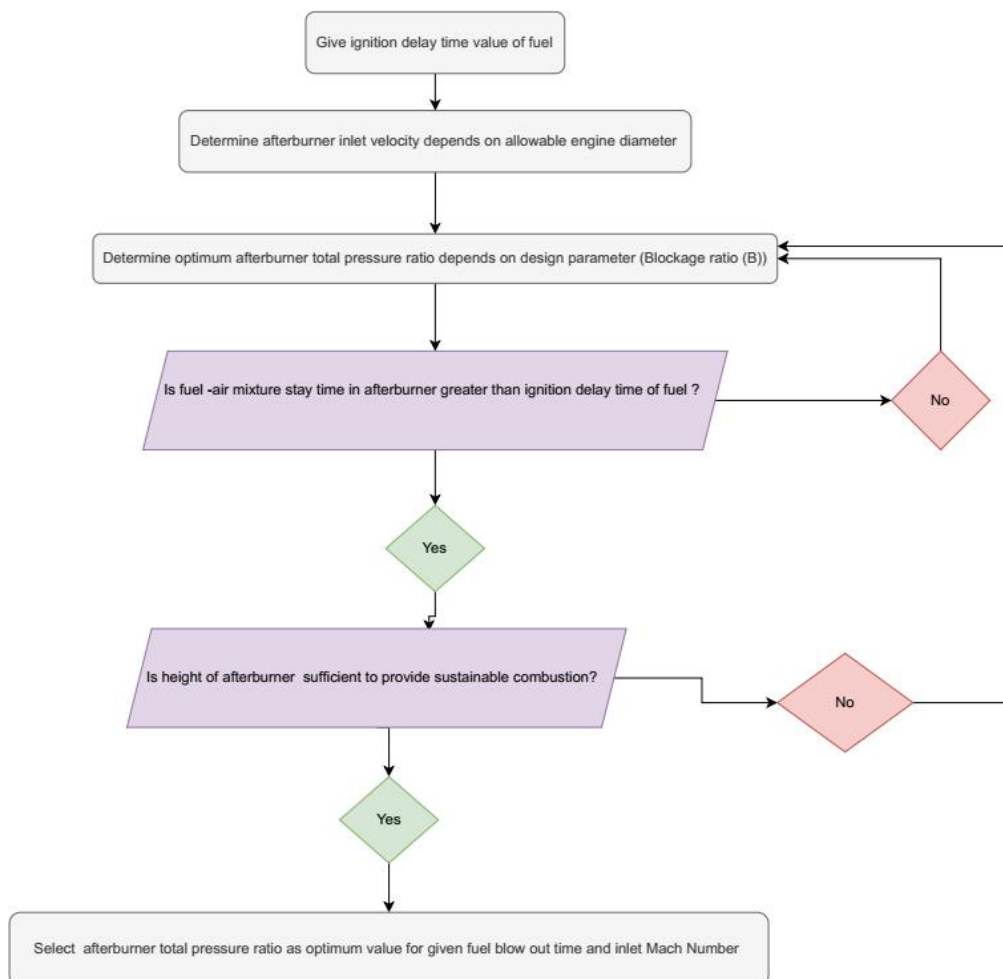


Fig. 2. Afterburner optimization algorithm.

The design approach is applied according to the afterburner optimization algorithm created in Figure 2.



3. Afterburner Conceptual Design

3.1. Calculations and theoretical modelling

The afterburner system schematic view is shown in Figure 3.

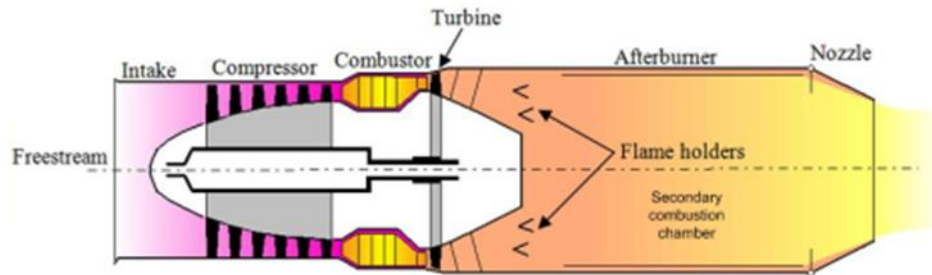


Fig. 3. Afterburner jet engine schematic view.

Jet A fuel is used as fuel in the afterburner design.

Table 2. Jet A fuel properties.

Property	Value
Chemical Formula	$C_{8.60}H_{17.27}$
Molecular Weight [kg/kmol]	120.678
Heat Value [MJ/kg]	43.10

The combustion reaction of JET A assuming complete combustion reaction is expressed below.

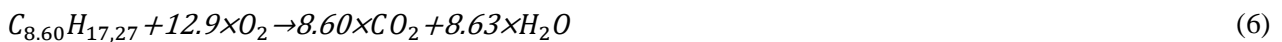


Table 3. Molecular weights of reactants entering the afterburner.

Molecule	Molecular Weight
$C_{8.60}H_{17.27}$	120.67 [kg/kmol]
O_2	15.999 [kg/kmol]
CO_2	44.01 [kg/kmol]
H_2O	18.01528 [kg/kmol]
N_2	14.0067 [kg/kmol]

The mass change in the gas composition as a result of combustion of a unit amount of fuel is summarized in Table 3 in terms of molecular weight values and in Table 4 in terms of fuel flow rate depending on the chemical equation expressed in the combustion reaction. It is assumed that nitrogen does not participate in the chemical reaction.

Table 4. Afterburner outlet gas composition mass fraction.

Molecule	Afterburner Exit Gas Composition
	Mass Ratio
O_2	0.0328
CO_2	0.1740
H_2O	0.0734
N_2	0.7234



Table 5. Afterburner inlet and outlet gas properties.

Gas Composition Characteristics	Value	
	Afterburner Inlet	Afterburner Exit
y [-]	1.3126	1.2519
R [J/kg. K]	282.7543	274.5904
c_p [J/kg. K]	1187.3	1364.7
MW [kg/kmol]	29.4036	30.2778

The gas composition of the core gas reacting in the primary combustion chamber at the exit of the turbine is given in Table 1. The molar characteristics of the reactants that will enter the combustion process per second are obtained, and the mass ratios from the reaction with Jet A fuel are computed since this gas composition is supplied in molar ratios. The fuel flow rate is calculated according to the algorithm expressed in Figure 4.

Table 6. Mass variation of combustion products depending on fuel flow rate.

Molecule	Gas Composition Mass Change
O_2	$-3.4312 \times m_{fuel}$
CO_2	$+ 3.1410 \times m_{fuel}$
H_2O	$+ 1.2901 \times m_{fuel}$
N_2	Not Change

Table 7. Afterburner inlet gas mass fraction.

Molecule	Mass Ratio
	Afterburner Inlet Gas Composition
O_2	0.1628
CO_2	0.0623
H_2O	0.0244
N_2	0.7505

Table 8. Molar properties of the substances to be involved in the combustion reaction.

Molecule	\dot{m} / \dot{m}_T	\dot{m} [kg/s]	\dot{n} [\dot{m}/MW]
O_2	0.1628	0.58608	0.0183
N_2	0.7504	2.70144	0.00596
H_2O	0.0244	0.08784	0.004876
CO_2	0.0623	0.22428	0.09643

In the combustion reaction, the equilibrium is regulated according to the amount of 0.0183 kmol/s O_2 . Accordingly, 0.000976 kmol of kmol $C_8H_{17,60}$, H_2O , N_2 and CO_2 enter the reaction. The calculation of the mass flow rate of $C_{12}H_{23}$ entering the reaction is expressed in the above equation.

$$\dot{m}_{C_{8,60}H_{17,60}} = \dot{n}_{C_{8,60}H_{17,60}} \cdot MW_{C_{8,60}H_{17,60}} = 0.000976 * 167.31 = 0.1632 \text{ kg/s} \quad (7)$$

$$\dot{m}_{C_{12}H_{23}} = 0.1632 \text{ kg/s} \quad (8)$$

Fuel to air ratio, f_{AB} , can be found as:

$$f_{AB} = \frac{\dot{m}_{C_{8,60}H_{17,60}} = 0.1632 \text{ kg/s}}{\dot{m}_{gaz=3.6} \text{ kg/s}} = 0.0453 \quad (9)$$

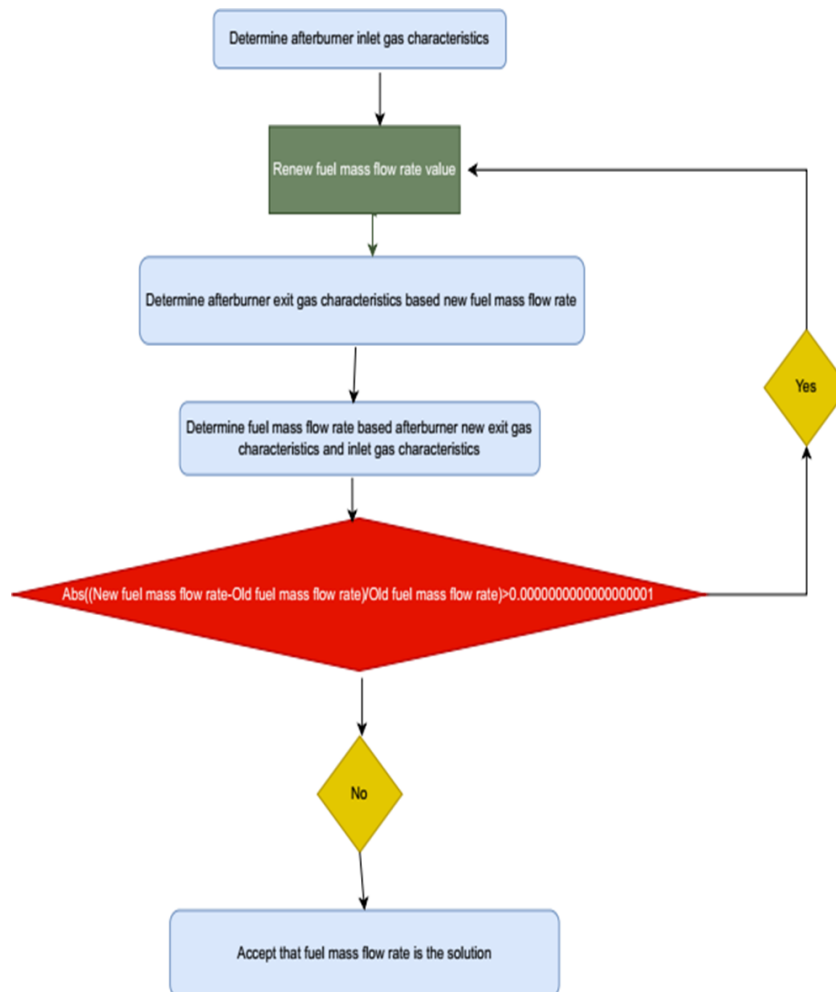


Fig. 4. Algorithm used to calculate fuel mass flow rate.

3.2. Design and modelling of geometric components

Figure 5 shows some of the main parts of the afterburner.

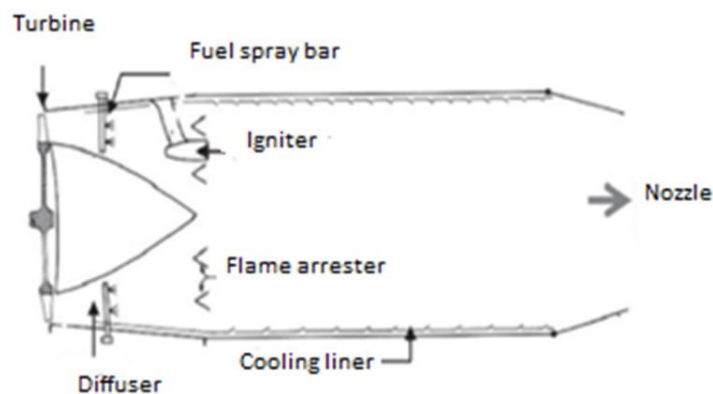


Fig. 5. Main features of a typical afterburner.



3.2.1. Diffusers

A diffuser is a diverging passage device in which the flow is slowed down and a decrease in the velocity of the flow head occurs. The reduction in velocity loads is converted into an increase in static pressure. Reducing the flow velocity at the diffuser exit to the appropriate value is how the exhaust diffuser, one of the key parts of the afterburner, stabilizes the flow. The total pressure loss has a significant impact on the thrust of the engine. Generally, one percent increase in overall pressure loss corresponds to one percent less thrust. A diffuser that can accomplish the necessary speed decrease in the least amount of time, with the least amount of overall pressure loss, and with a consistent and steady flow state at the exit is considered optimal from the perspective of the designer. Due to the afterburner's fuel injection systems and flame arrester blocking the flow, large deflection angles can be employed to lessen the flow's inclination to exit the diffuser cone. A library of the AEDSYS software [25], AFTRBNR [25], is used for diffuser geometry calculation.

Table 9. Station parameters.

Station 6A			
Mach number	Diffuser inlet total pressure	Inlet flow mass flow rate	Diffuser inlet total temperature
0.4274 [-]	300 [kPa]	3.6 [kg/s]	1050 [K]
Station 6.1			
Fuel mass flow rate		Diffuser external diameter	
0.163 [kg/s]		8.5 [cm]	
Station 7			
After Vee-gutter total pressure		After Vee-gutter total temperature	
260 [kPa]		2000 [K]	

Station 6A core engine exit and afterburner inlet parameter values are the diffuser geometry calculation design point values. Figure 6 shows the diffuser geometry detail parameters.

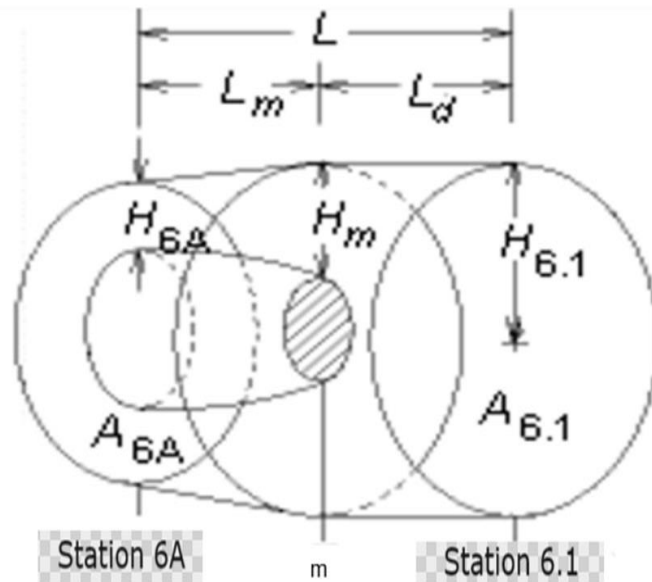
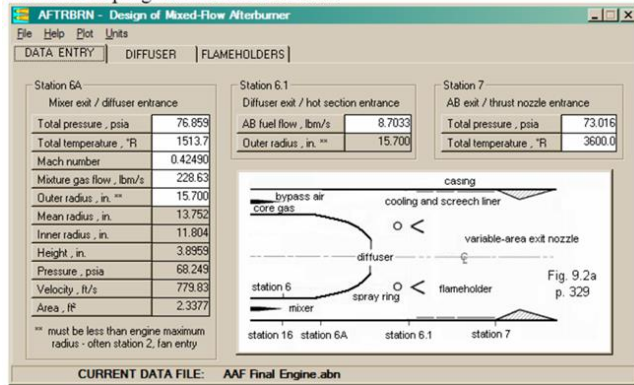


Fig. 6. Geometric parameters of diffuser.

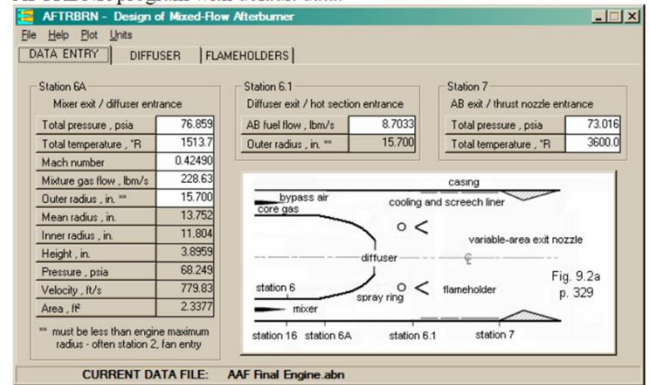
If the input parameters are entered into the AFTRBNR [25] program, the library of the AEDYS [25] program, the performance values and dimensions given in Table 10 and Table 11 are obtained.



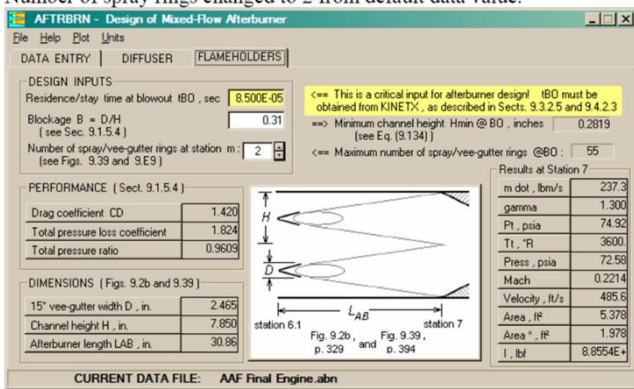
AFTRBNR program with default data.



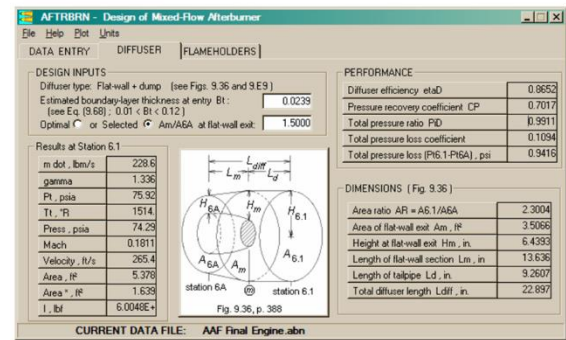
AFTRBNR program with default data.



Number of spray rings changed to 2 from default data value.



User selected diffuser area ratio set to 1.5 from optimal to reduce length of diffuser.



Sketch of resulting cross-section.

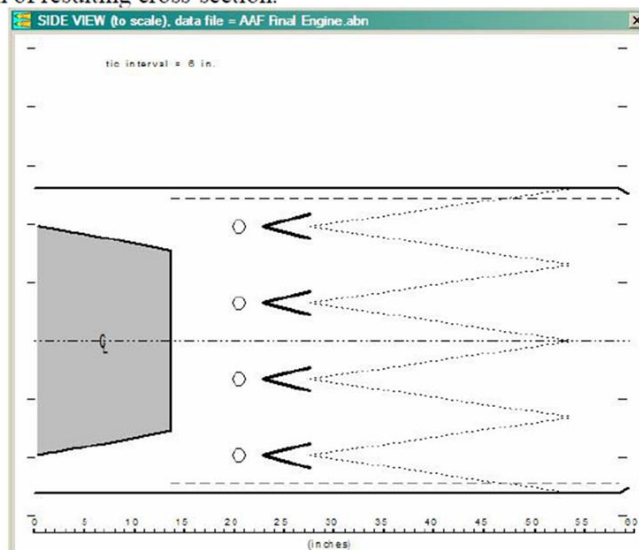


Fig. 7. Geometric parameters of diffuser.



Table 10. Diffuser performance.

Parameter	Value
Diffuser efficiency [-]	0.816
Pressure coefficient change [-]	0.4970
Total pressure ratio [-]	0.987
Total pressure loss coefficient [-]	0.111
Total pressure loss [Pa]	799

Table 11. Diffuser dimensions.

Dimension	Value
Area ratio [-]	1.59
Diffuser area [m^2]	0.0175
Diffuser height [cm]	4.4645
Diffuser centre length [cm]	7.3887
Diffuser tip length [cm]	4.0355

The designed diffuser geometry is displayed in Figure 8. The selection of elliptical geometry minimizes flow separation.

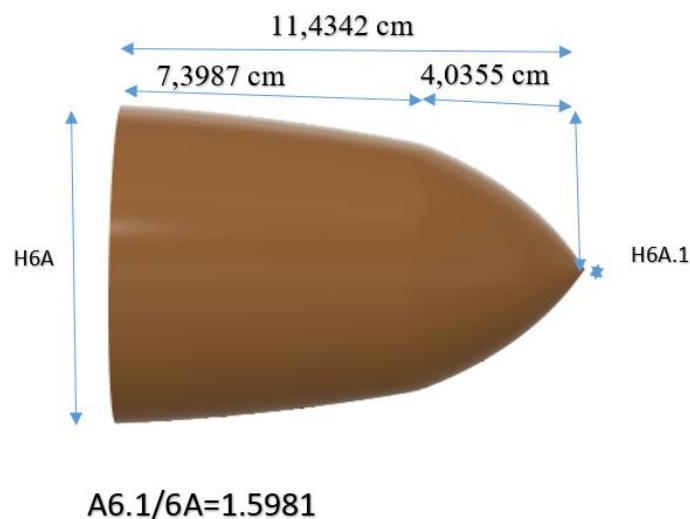


Fig. 8. Diffuser geometry parameters.

3.2.2. Fuel spray bars

Fuel injection bars typically consist of one or more rings with different fuel injection heads distributed circumferentially around the ring. Radial spray bars are the type of injection system in use. Slightly above the flow, these bars can be found. To smooth the flow after the turbine, they are integrated into a single cantilever inside the diffuser. A distinct advantage of radial spray bar systems is that they can be easily removed for inspection and both parameters of number and hole position can be easily changed.

The fuel spray bars are evenly spaced circumferentially. They are in a single axial plane across the combustion chamber or diffuser. The fuel injector array consists of stub pipes mounted radially on circular manifolds. In Figure 9, the orifice diameter of the fuel injection bars is 0.635 centimetres. (0.25 inch). In the downstream position there are 24 nozzle bar assemblies spaced at 15-degree intervals. The downstream nozzle bars are located 4 centimetres above the flame arrester face.

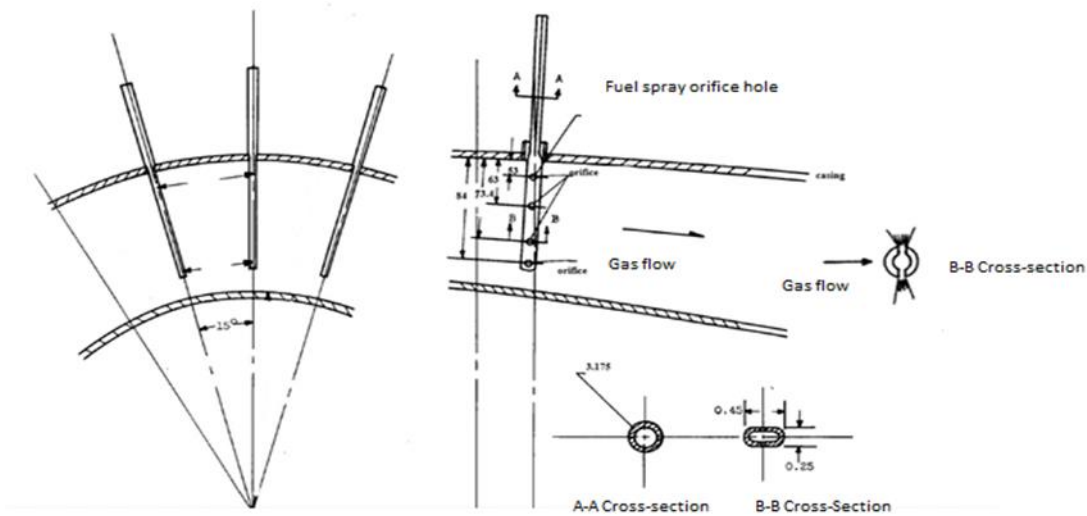


Fig. 9. Spray bar position configuration.

Parameter values for afterburner spray bar configuration are expressed in the table below.

Table 12. Afterburner spray bar configuration information.

Manifold Type	Number of holes in the bar	Hole diameter [cm]	Injection position
24 radial bars	8	0.0635	Core, downstream

Figure 9 shows the installation of the manifold and spray bars.

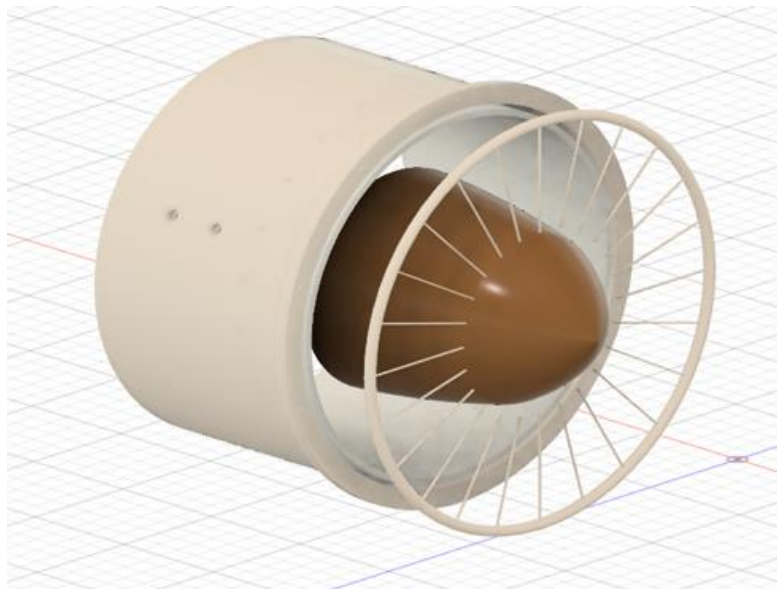


Fig. 10. 3D spray bar view.

An engine such as a rocket or jet uses a flame arrester to maintain combustion. To keep the flame from going out and allow the fuel to continue burning continuously to produce thrust, a tiny area of reduced efficiency is created. A classic flame arrester consists of a cylinder with some air holes inside to allow air to swirl. Air currents passing through the engine swirl around the device, leaving a space in the centre where a flame can burn. As the fuel burns, the air around the flame holder raises its temperature. As the rapidly heated air expands to create thrust, the high heat ignites the incoming fuel, keeping the engine running continuously. As shown in Figure 11, the fuel particles



return to the vee-gutter in the circulation zone and stay longer in the reaction zone, which means longer residence time. The incoming gas supplies oxygen to the reaction zone and a stationary flame is formed at a point after the V-nozzle. The flame necessarily spreads along the afterburner and convergent-divergent nozzles. One of the main problems of vee-gutter is blocking the flow. If the blockage increases, it leads to a higher drag coefficient (C_d) and total pressure loss. The design of the vee-gutter should have an optimum blockage value. The guiding part in this section is drag coefficient and pressure loss. It is aimed to determine the Vee-gutter design by paying attention to the relevant parameters. Considering intensive research and previous experiments, the number, angle and position of the Vee-gutter are determined in the study.

Table 13. Vee-gutter design parameters.

Parameter	Value
Blow out time [s]	6.29×10^{-5}
Blockage ratio [-]	0.314
Number of Vee-gutter rings [amount]	2

KINETIX, a library of AEDSYS software, is used for vee-gutter geometry calculation.

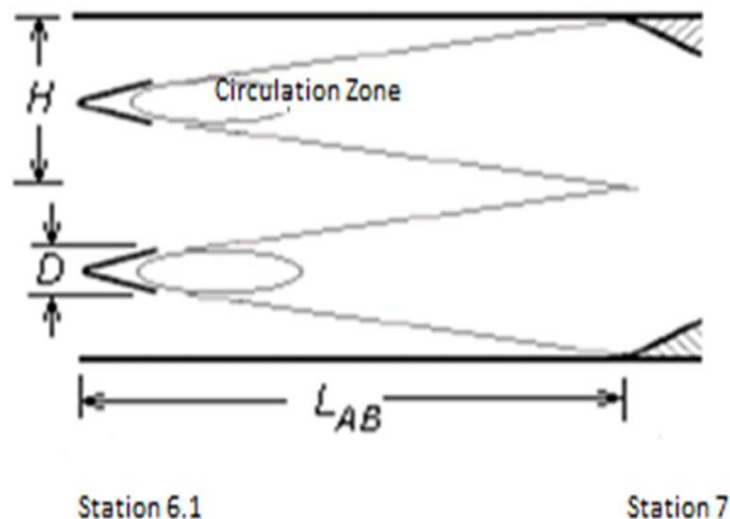


Fig. 11. Typical vee-gutter configuration.

By entering the pre-calculated and determined design parameters into the developed AFTRBNR software [25], we can see the performance, dimensioning and characteristics of the flow leaving the vee-gutter. Commercial computational fluid dynamics software can be used for more precise solution.

Table 14. Vee-gutter performance parameters.

Parameter	Value
Drag coefficient	1.42
Total pressure loss coefficient	1.35
Total pressure ratio	0.939



Table 15. Vee-gutter dimensions.

Parameter	Value
Vee-gutter height [cm]	1.335
Afterburner channel height [cm]	42.50
Afterburner channel length [cm]	28.14

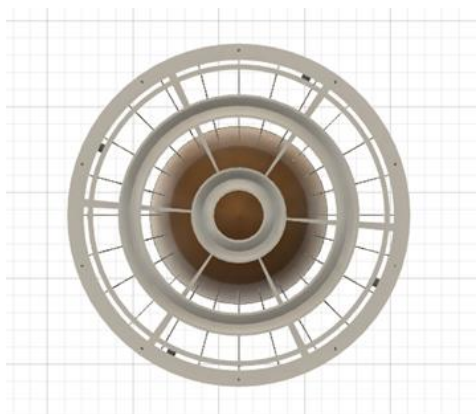


Fig. 12a. Vee-gutter 3D front view.

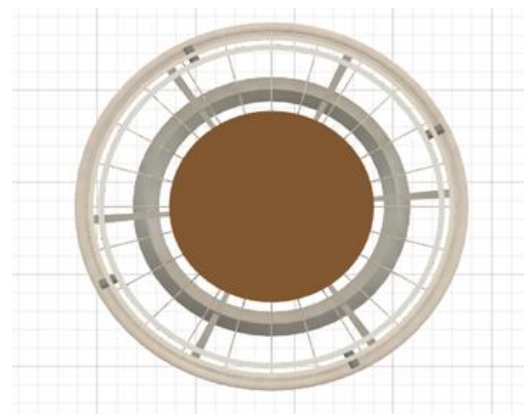


Figure 12b. Vee-gutter 3D back view.

3.3. Final design

The technical drawing of the afterburner is shown in Figure 12. The afterburner design shown in Figure 12 is investigated using computational fluid dynamics for unreacted flow. The performance parameters of the reacted flow are investigated using 1-D analytical calculations and AFTRBNR software [25], which is the library of AEDSYS software [25].

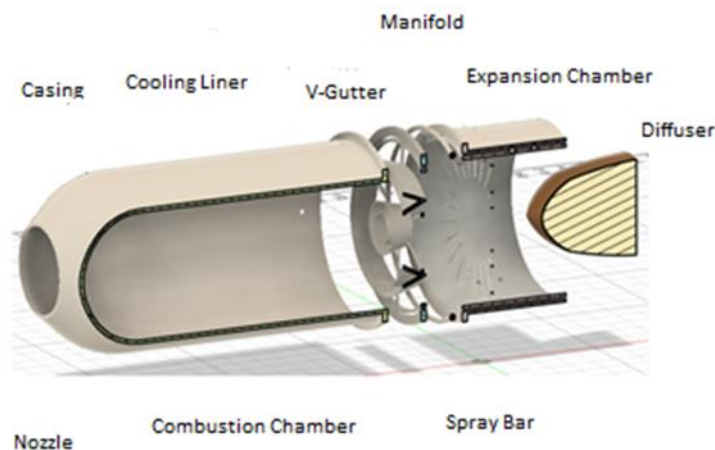


Fig. 13. Afterburner components.

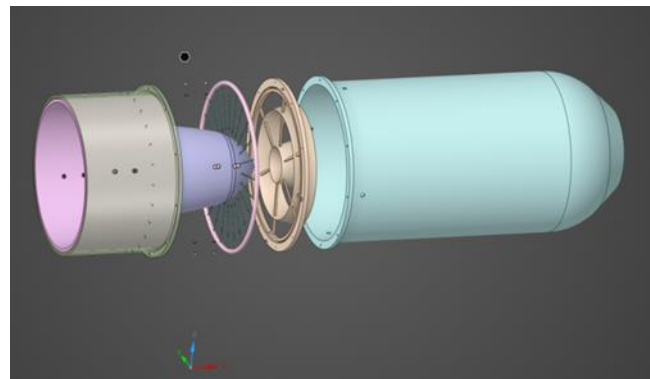


Fig. 14. Afterburner final design.

6. CFD Analyses

6.1. Methods and parameters used in numerical modelling

The aim of this study is to perform two-dimensional axisymmetric calculations in an afterburner combustion chamber. An advanced CFD (Computational Fluid Dynamics) software based on an unstructured grid is used to perform the calculations using the density-based finite volume method [27]. The standard "k-ε" model is applied to calculate turbulent flow characteristics. The standard "k-ε" model is a high Reynolds model and is not valid in regions close to the wall where viscous effects dominate the effects of turbulence. Instead, wall functions are used in cells adjacent to walls. The mathematical models used to simulate the combustion of Jet A fuel in the afterburner are fully compressible transient Reynolds-averaged Navier-Stokes equations and spatially filtered fully compressible transient Navier-Stokes equations, CFX-11 (CFD) code provided by ANSYS™ [27] is used to perform commercial fluid dynamics simulations.

Due to the symmetry of the geometry, a 60° sector is modelled.

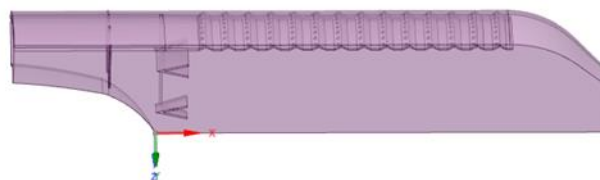


Fig. 15 Afterburner 60-degree sector model.

6.2. Combustion turbulence modelling

The "k-ε" is a two-equation turbulence model. This model is widely used. Because it offers a good compromise between numerical effort and computational accuracy. This model uses the gradient diffusion hypothesis to relate the Reynolds stresses to the mean velocity. As gradients and turbulence viscosity. Turbulent viscosity is modelled as the product of turbulent velocity and turbulent length scale. In the "k-ε" model, the turbulent velocity scale is calculated from the turbulent kinetic energy provided from its solution.

The high Reynolds number form of the k-ε equation is as follows:

$$\frac{\partial(p \times u \times \kappa)}{\partial x} + \frac{\partial(p \times v \times \kappa)}{\partial y} = \frac{\partial \left(\frac{\mu_T}{\sigma_\kappa} \times \frac{\partial \kappa}{\partial y} \right)}{\partial y} + P_\kappa - p \times \epsilon \quad (10)$$



$$\frac{\partial(p \times u \times \varepsilon)}{\partial x} + \frac{\partial(p \times v \times \varepsilon)}{\partial y} = \frac{\partial\left(\left(\frac{\mu_T}{\sigma_\varepsilon}\right) \times \frac{\partial \varepsilon}{\partial y}\right)}{\partial y} + c_1 \times \frac{\varepsilon}{\kappa} \times P_\kappa - c_2 \times p \times \frac{\varepsilon^2}{\kappa} \quad (11)$$

where

$$\mu_T = c_\mu \times p \times \frac{\kappa^2}{\varepsilon} \quad (12)$$

$$P_\kappa = \mu_T \times \left(\frac{\partial u}{\partial y}\right)^2 \quad (13)$$

The low Reynolds number form of the model:

$$\frac{\partial(p \times u \times \kappa)}{\partial x} + \frac{\partial(p \times v \times \kappa)}{\partial y} = \frac{\partial\left(\left(\mu + \frac{\mu_T}{\sigma_\kappa}\right) \times \frac{\partial \kappa}{\partial y}\right)}{\partial x} + P_\kappa - p \times \varepsilon - \mu \times \left(\frac{\partial \sqrt{\kappa}}{\partial y}\right)^2 \quad (14)$$

$$\frac{\partial(p \times u \times \varepsilon)}{\partial x} + \frac{\partial(p \times v \times \varepsilon)}{\partial y} = \frac{\partial\left(\left(\mu + \frac{\mu_T}{\sigma_\varepsilon}\right) \times \frac{\partial \varepsilon}{\partial y}\right)}{\partial y} + c_1 \times \frac{\varepsilon}{\kappa} \times P_\kappa - c_2 \times f_2 \times p \times \frac{\varepsilon^2}{\kappa} + 2 \times \mu \times \mu_T \times \left(\frac{\partial^2 u}{\partial y^2}\right)^2 \quad (15)$$

where

$$Re_T = \frac{p \times \kappa^2}{\mu \times \varepsilon} \quad (16)$$

$$f_2 = 1.0 - 0.3 \times \exp(-Re_T^2) \quad (17)$$

The turbulent length scale is estimated from two properties. The turbulence field is usually derived from the turbulent kinetic energy and the dissipation rate, while the dissipation rate of turbulent kinetic energy is derived from the solution of its transport.

Mesh dependency study was performed with respect to Mach number at the nozzle exit and velocity values. Mesh number of elements was changed from 2.5x10⁶ to 6.0x10⁶, as seen in Table 16. Computation time and variation values were taken into account and mesh number was arranged as 4.0x10⁶ for detail CFD analysis due to becoming nearly asymptotic variation of the values.

With the basic geometry corrected and ready for simulation, the next step is to mesh the geometry. The first mesh is made according to the default settings in ANSYS Meshing [27]. The first mesh of the whole area can be seen in Figure 16.

Table 16. Variation of Mach number and velocity at the nozzle exit depending on mesh number.

Mesh number	Ma at nozzle exit	Velocity at nozzle exit (m/s)
6.0x10 ⁶	1.4376	684.39
5.0x10 ⁶	1.4371	684.33
4.0x10 ⁶	1.4367	684.24
3.5x10 ⁶	1.4353	683.90
3.0x10 ⁶	1.4337	683.85
2.5x10 ⁶	1.4313	683.67

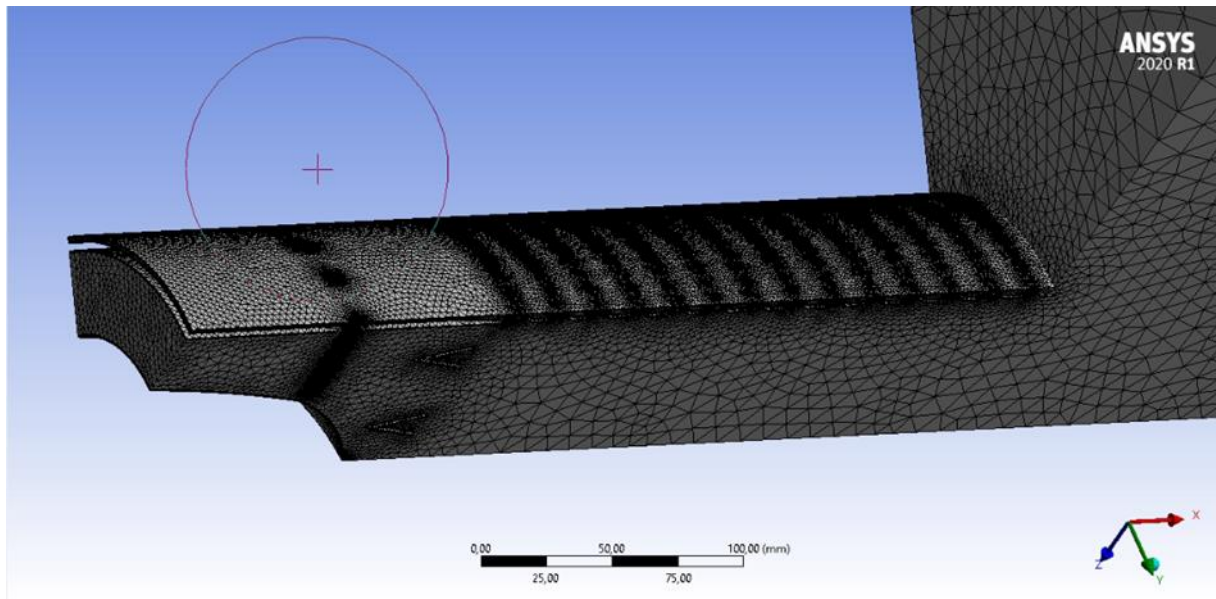


Fig. 16 Afterburner mesh model and mesh statistics.

7. Unreacted Flow Analysis Results

Figure 17 shows a plot of the velocity distribution over the entire afterburner from the inlet to the nozzle outlet. The flow along the diffuser passage slows down after passing over the spray bars. The supports, fuel spray bars and vee-groove obstruct the flow and cause low velocity zones to form behind them. The velocity in the combustion zone is relatively low due to the obstruction created by the vee-groove. As expected, there is a significant increase in velocity in the divergent part of the convergent-divergent (CD) nozzle. Table 16 shows the mass-weighted average axial velocity and Mach number in various regions of the afterburner. The average Mach number at the core inlet mass is assumed to be 0.47 and at the end of the exhaust diffuser the Mach number is reduced to 0.22. The average Mach number at the nozzle inlet plane is about 0.26 and increases to 1.5 at the nozzle outlet plane. The flow in the bypass starts at Mach number 0.1 and gradually mixes with the core air through the chute, screech holes, cooling ring holes and nozzle. The overall mass-weighted total pressure loss (from afterburner inlet to the convergent-divergent nozzle exit) is about 9.2%.

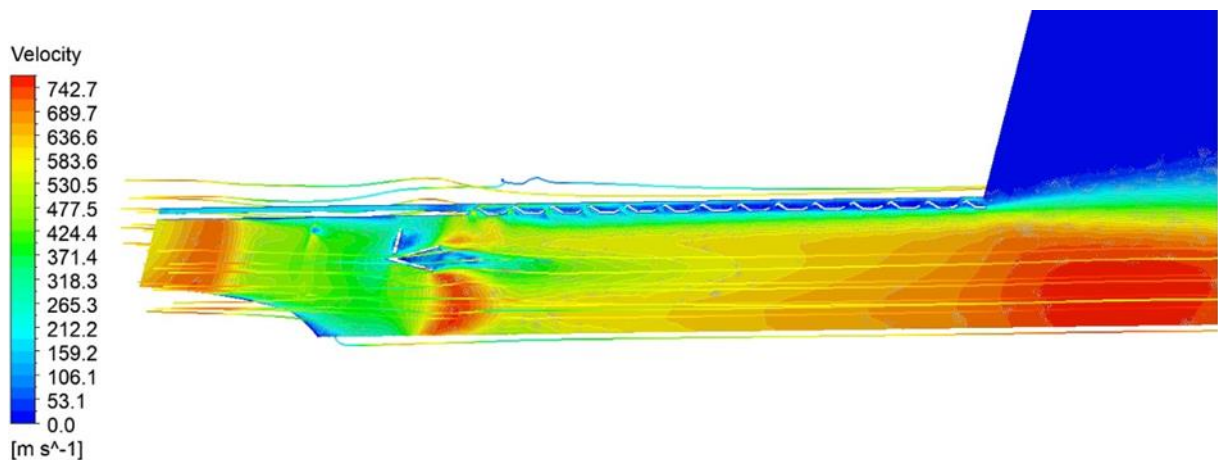


Fig. 17 Mid-plane velocity distribution of afterburner.



The mass-averaged axial velocity and Mach number in various regions of the afterburner for unreacted conditions are given in Table 17.

Table 17. Mach number and velocity for unreacted flow.

Region	Mach Number	Velocity [m/s]
Bypass channel inlet	0.1700	76
Diffuser exit	0.2800	165
Nozzle inlet	0.3400	201
Nozzle exit	1.4367	684

The mass-averaged Mach number is 0.44 at the core inlet and is reduced to 0.28 at the diffuser exit. It is 0.34 at the nozzle inlet and increases to 1.4367 at the nozzle exit. The flow at the bypass starts with a Mach number of 0.17 and gradually mixes with the core air through the chute, sound holes, cooling ring holes and nozzle. Figure 18 shows the total pressure distribution. The pressure decreases from 720 kPa to 27.3 kPa due to the expansion.

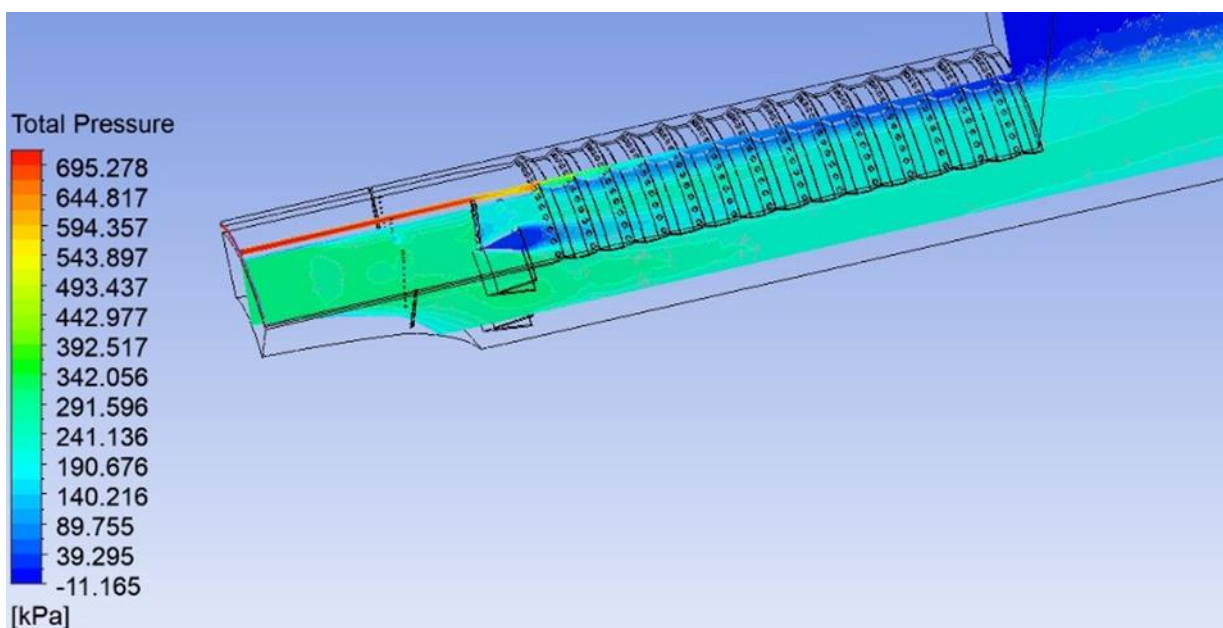


Fig. 18 Total pressure contours.

Much less change in static temperature is found. The flow temperature decreases towards the rear, probably due to mass flow entrainment from the bypass duct. Figure 19 shows the total temperature contours in different sections along the afterburner. The flame is anchored behind the vee-groove and continues in the direction of the high temperature zone. The flame at the rear of the vee-gutter provides a constant ignition source and provides anchorage to the downward flowing fuel-air mixture.

The maximum temperature observed behind the vee-gutter is about 1050 K. The total temperature spread increases downstream of the vee-gutter up to the nozzle inlet.

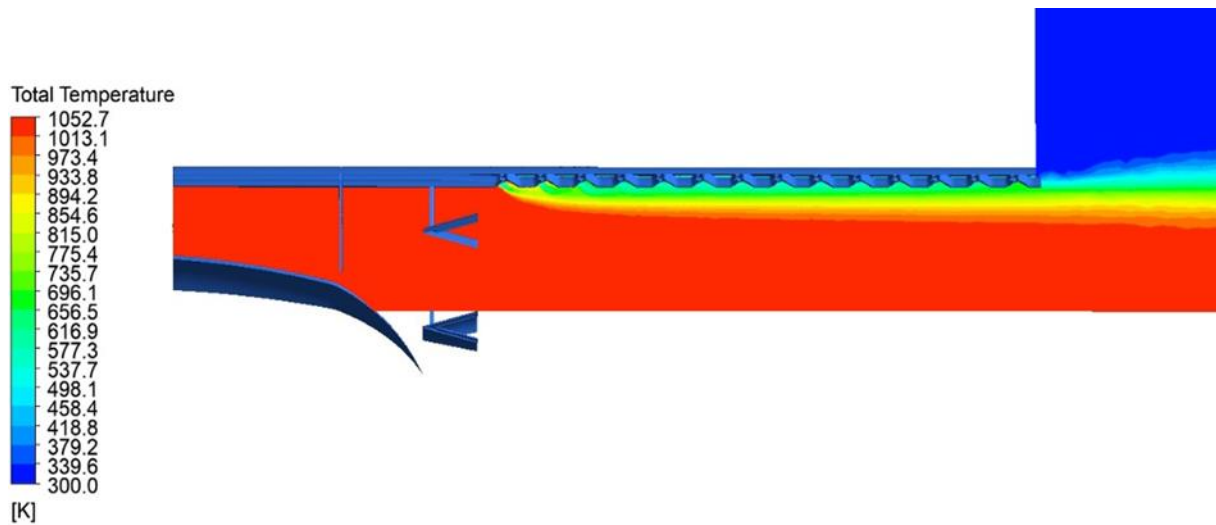


Fig. 19 Total cold and hot flow mixture temperature contours.

8. Determination of Reacting Flow

Under reacting flow conditions, the nozzle throat and exit area are increased so that the conditions of the afterburner inlet state and the upstream components of the afterburner do not change due to the combustion. This prevents any increase in backpressure build-up that would slow down the airflow in the engine and affect the stall characteristics of the compressor. The flame is anchored behind the vee-gutter and the high temperature zone continues in the direction of the nozzle. The flame behind the vee-gutter provides a constant ignition source and spreads the flame from these sources into the fuel air mixture as it flows downstream. It is clearly seen that the total temperature spread increases along the afterburner length. The total temperature increases from the vee-gutter towards the nozzle inlet. There is a small decrease in the total temperature at the nozzle inlet due to bypass flow mixing. The increase in temperatures along the afterburner significantly increases the velocity of the gases to achieve the required thrust.

Afterburner performance is evaluated in terms of total pressure loss, thrust/thrust boost and combustion efficiency. Inlet mixture, total pressure and total temperature are calculated using mass flow average values. The components affecting the pressure loss and their effect values are given in the table below.

Table 18. Loss factors effected total pressure losses.

Loss Factor	Total Pressure Ratio
Diffuser	0.9873
Vee-Gutter	0.9390
Temperature Increase	0.9000
Nozzle	0.9800

$$P_{t7} = P_{t6} \times H_{AB} \tag{18}$$

$$P_{t8} = P_{t7} \times H_{nozzle} \tag{19}$$

$$P_{t9} = P_{t8} \times H_{st} \tag{20}$$

Total pressure loss value is calculated as 14.96%.

Equations used in the calculation of thrust are expressed below:

$$M_9 = \sqrt{\frac{2}{\gamma - 1} \left[\left(\frac{P_{t9}}{P_9} \right)^{\frac{\gamma - 1}{\gamma}} - 1 \right]} \tag{21}$$



$$T_9 = \frac{T_{t9}}{1 + \frac{\gamma-1}{2} M_9^2} \tag{22}$$

$$a_9 = \sqrt{\gamma \times R \times T_9} \tag{23}$$

$$V_9 = M_9 \times a_9 \tag{24}$$

$$T = (\dot{m}_6 + \dot{m}_f) \times V_9 \tag{25}$$

The parameters required for thrust calculation are given in Table 19.

Table 19. Design parameter values.

Parameter	Value
P_{t9} [kPa]	255.12
P_9 [kPa]	101.325
T_{t9} [K]	2000
γ [-]	1.3
R [J/(kg.K)]	229
\dot{m}_9 [kg/s]	3.6
\dot{m}_f [kg/s]	0.1623

As a result of the calculation, the afterburner thrust value is 3284.53 N. The calculated thrust value without afterburner is 2985 N. It was observed by the analysis under 1-D and unreacted flow that the thrust increase by using afterburner was 10.1%. It is shown that much better results can be obtained in thrust increase by stabilizing the performance parameters.

It is a measure of the ability to completely burn the fuel inside the afterburner. Combustion efficiency is calculated based on the actual total temperature rise leading to the ideal temperature rise. The ideal temperature rise is calculated from the AEDSYS software [25]. The actual total temperature is obtained from CFD analysis at the nozzle outlet of the afterburner. The program inputs are in Table 20. Afterburner combustion efficiency design parameters are given in Table 21. Afterburner performance parameters is presented in Table 22.

Table 20. Core flow inlet gas composition values molar ratio values.

Molecule	Molar Ratio
O_2	5.0540×10^{-3}
N_2	2.6620×10^{-3}
H_2O	1.3480×10^{-3}
CO_2	1.406×10^{-3}

Table 21. Afterburner combustion efficiency design parameters.

Parameter	Value
Area [cm^2]	226.98
Length [cm]	28.14
Fuel Mass Flow Rate [kg/s]	0.1632
Mass Flow Rate [kg/s]	3.6
Jet A Heat Value [MJ/kg]	43.031
Total Pressure [kPa]	300
Total Temperature [K]	1050



Table 22. Afterburner performance parameters.

Parameter	Value
Blowout Time [s]	6.4687×10^{-5}
Residence Time [s]	8.5642×10^{-5}
Combustion Efficiency [-]	0.815
Afterburner Exit Total Temperature [K]	2044

The combustion efficiency is approximately 81.5%. It is observed that the blowout time obtained because of the calculations is more than the time required for the reaction time to be in the afterburner and flame stabilization is achieved.

9. Conclusion

An afterburner is conceptually designed within the existing geometrical constraints to minimize the damage to the existing engine geometry. Analytical performance evaluation is performed using 1-D analytical calculations and unreacted flow analysis. Afterburner is designed with 81.5% combustion efficiency. Drag coefficient of afterburner is 1.42, total pressure loss coefficient of afterburner is 1.35 and total pressure ratio of afterburner is 0.939. Vee-gutter height of afterburner designed is 1.335 cm, channel height is 42.50 cm, channel length 28.14 cm. It is observed that a 10.1% gain in net thrust was achieved by using an afterburner at expense of 50% increase specific fuel consumption. This gain can be very useful for any unmanned air vehicle in hostile conditions for take-off with extra load and manoeuvring and ditching. Afterburner reacting flow analytical CFD combustion analyses are in progress. Real time performances of any combustor can only be obtained by testing and hence testing of the proposed design is recommended. The outputs of the designed 3-D model (reacting flow) can be generated using computational fluid dynamics simulation programs in future.

Authorship contribution statement for Contributor Roles Taxonomy

Muhammed Cuma Sönmez: Software, Methodology, Writing- Reviewing and Editing, Validation; **Mustafa Karabacak:** Conceptualization, Methodology, Writing- Reviewing and Editing, Validation; **Muammer Özgören:** Supervision, Conceptualization, Writing- Reviewing and Editing. The corresponding author, **Mustafa Karabacak**, is responsible for ensuring that the descriptions are accurate and agreed by all authors.

Conflicts of Interest: The authors declare no conflict of interest.



References

- [1] Krishnan, G., Paulo, C., & Maris, D. N. 2013. An assessment of relative technology benefits of a variable pitch fan and variable area nozzle. In 49th AIAA/ASME/SAE/ASEE Joint Propulsion Conference (p. 3604).
- [2] Breton, J. J., Huff, D. L., Geiselhart, K., & Seidel, J. 2020. Supersonic technology concept aero planes for environmental studies. In AIAA SciTech 2020 Forum (p. 0263).
- [3] Hendricks, E. S., Flack, R. D., & Gray, J. S. 2017. Simultaneous propulsion system and trajectory optimization. In 18th AIAA/ISSMO Multidisciplinary Analysis and Optimization Conference (p. 4435).
- [4] McGrew, J. S., How, J. P., Williams, B., & Roy, N. 2010. Air-combat strategy using approximate dynamic programming. *Journal of guidance, control, and dynamics*, 33(5), 1641-1654.
- [5] Ashley, S. 1995. Thrust vectoring: a new angle to air superiority. *Mechanical Engineering*, 117(1), 58.
- [6] Rumsfeld, D. H. 2002. Transforming the military. *Foreign Off.*, 81, 20.
- [7] Tam, C. K. 2021. On the generation of entropy noise in a shock containing nozzle of high-performance aircraft at afterburner. *Journal of Sound and Vibration*, 512, 116389.
- [8] Williams, J., & Ezunkpe, Y. 2023. Design of an Efficient Turbofan Engine with Afterburners. *Journal of Engineering and Applied Sciences Technology*. SRC/JEAST-248. DOI: doi.org/10.47363/JEAST/2023 (5), 177, 2-8.
- [9] Xing, F., Kumar, A., Huang, Y., Chan, S., Ruan, C., Gu, S., & Fan, X. (2017). Flameless combustion with liquid fuel: A review focusing on fundamentals and gas turbine application. *Applied Energy*, 193, 28-51.
- [10] Tamarin, Y. 2002. Protective coatings for turbine blades. ASM international.
- [11] Liu, S., Li, J., Zhu, G., Wang, W., & Liu, Y. (2018). Mixing and combustion enhancement of turbocharged solid propellant ramjet. *Acta Astronautica*, 143, 193-202.
- [12] Carter, P., & Balepin, V. 2002. Mass injection and precompressor cooling engines analyses. In 38th AIAA/ASME/SAE/ASEE Joint Propulsion Conference & Exhibit (p. 4127).
- [13] Xu, L., Sun, Z., Ruan, Q., Xi, L., Gao, J., & Li, Y. 2023. Development Trend of Cooling Technology for Turbine Blades at Super-High Temperature of above 2000 K. *Energies*, 16(2), 668.
- [14] Gurrappa, I., Yashwanth, I. V. S., Mounika, I., Murakami, H., & Kuroda, S. 2015. The importance of hot corrosion and its effective prevention for enhanced efficiency of gas turbines. *Gas Turbines-Materials, Modeling and Performance*, 1, 55-102.
- [15] Chen, F., Ruan, C., Yu, T., Cai, W., Mao, Y., & Lu, X. 2019. Effects of fuel variation and inlet air temperature on combustion stability in a gas turbine model combustor. *Aerospace Science and Technology*, 92, 126-138.
- [16] Burger, V. 2017. The influence of fuel properties on threshold combustion in aviation gas turbine engines.
- [17] Safdar, M. M., Masud, J., Mufti, B., Naseer, H. U., Farooq, A., & Ullah, A. 2020. Numerical Modeling and Analysis of Afterburner Combustion of a Low Bypass Ratio Turbofan Engine. In AIAA Scitech 2020 Forum (p. 0628).
- [18] Ebrahimi, H. 2006. Overview of gas turbine augmentor design, operation, and combustion oscillation. In 42nd AIAA/ASME/SAE/ASEE Joint Propulsion Conference & Exhibit (p. 4916).
- [19] Anand, R., Lokesharun, D., Rajkumar, S., & Kirubakaran, R. 2017. 3D CFD analysis in an afterburner using NUMECA. *IJAREM*. ISSN, 2456-2033.
- [20] Davis Jr, M. W., & Kidman, D. S. 2010. Prediction and analysis of inlet pressure and temperature distortion on engine operability from a recent T-38 flight test program. In *Turbo Expo: Power for Land, Sea, and Air* (Vol. 43963, pp. 1-11).
- [21] Lovett, J., Brogan, T., Philippona, D., Kiel, B., & Thompson, T. 2004. Development needs for advanced afterburner designs. In 40th AIAA/ASME/SAE/ASEE joint propulsion conference and exhibit (p. 4192).



-
- [22] Lord, W., MacMartin, D., & Tillman, G. 2000. Flow control opportunities in gas turbine engines. In Fluids 2000 Conference and Exhibit (p. 2234).
- [23] Ebrahimi, H. 2006. Overview of gas turbine augmentor design, operation, and combustion oscillation. In 42nd AIAA/ASME/SAE/ASEE Joint Propulsion Conference & Exhibit (p. 4916).
- [24] Lovett, J., Brogan, T., Philippona, D., Kiel, B., & Thompson, T. 2004. Development needs for advanced afterburner designs. In 40th AIAA/ASME/SAE/ASEE joint propulsion conference and exhibit (p. 4192).
- [25] Mattingly, J. D. 2002. Aircraft engine design. AIAA.
- [26] Cooper, J., & Dingle, L. 2005. Engineering an afterburner for a miniature gas turbine engine. *Aircraft Engineering and Aerospace Technology*, 77(2), 104-108.
- [27] ANSYS Inc. 2020. Ansys Fluent User's Guide Release 2020 R1.